Tunnelling and Underground Space Technology 50 (2015) 465–478

Contents lists available at ScienceDirect

Tunnelling and Underground Space Technology

journal homepage: www.elsevier.com/locate/tust

Interaction between surface structures and tunnelling in sand: Centrifuge and computational modelling

Giorgia Giardina *, Matthew J. DeJong, Robert J. Mair

Department of Engineering, University of Cambridge, Trumpington Street, CB2 1PZ Cambridge, UK

ARTICLE INFO

Article history:
Received 28 November 2014
Accepted 13 July 2015

Keywords:
Centrifuge testing
Numerical modelling
Settlements
Soil–structure interaction
Tunnelling

ABSTRACT

Tunnelling in urban areas requires a careful estimation of the consequence of soil settlements on existing buildings. In this paper the interaction between the excavation of a tunnel in sand and surface structures is investigated. A two dimensional finite element model is presented and validated through comparison with centrifuge test results, both with and without structures. The model is then used to perform a sensitivity study on the effect of building weight on soil movements and structural deformations. The results of the validation indicate that assuming a no-tension interface between the soil and the structure is essential to capture the soil–structure interaction that was experimentally observed. The parametric analyses show that the relation between the building stiffness and the tunnelling-induced deformations depends on the building weight.

1. Introduction

Urban growth is continuously increasing and is expected to reach 60% in 2030 and 70% in 2050 (World Urbanization Prospects, 2014). One of the major challenges for expanding cities is the development of efficient and sustainable mobility. Rail and metro tunnels are an extensively adopted solution to address road congestion while minimising pollution. However, underground excavation causes soil settlement, which may affect surface structures. Tunnelling designs therefore require extensive assessment of potential settlement damage to existing buildings.

Standard procedures for the prediction of tunnelling-induced damage to surface masonry structures have been developed and applied (Mair et al., 1996). The core stage of these procedures assumes that predicted soil surface greenfield settlements caused by the excavation can be directly applied to a weightless and elastic beam that serves as a representative model of the building (Burland and Wroth, 1974; Burland et al., 1977; Boscardin and Cording, 1989; Burland, 1995). Total tensile strains of the equivalent beam are analytically derived and compared to critical values that determine the level of expected damage. The method has been recently extended to the third dimension (Namazi and Mohamad, 2013).

The original formulation of the critical tensile strain approach neglects soil–structure interaction. For this reason, a primary development of this method was the inclusion of the relative stiffness between the structure and the soil (Potts and Addenbrooke, 1997; Son and Cording, 2005; Franzius et al., 2006; Dimmock and Mair, 2008; Farrell, 2010; Goh and Mair, 2011). Other aspects have also be shown to affect the soil–structure interaction, including: the nonlinear behaviour of the building material (Boonpichetvong and Rots, 2005; Son and Cording, 2005; DeJong et al., 2008; Laefer et al., 2011; Nghiem et al., 2014; Giardina et al., 2012, 2013; Amorosi et al., 2014), the initial structural damage (BRE, 1995; Guglielmetti et al., 2008; Devriendt et al., 2013; Clarke and Laefer, 2014), the presence of large openings (Son and Cording, 2007; Melis and Rodriguez Ortiz, 2001; Pickhaver et al., 2010; Giardina et al., 2015b), the torsional behaviour of the building (Burd et al., 2000; Franzius et al., 2006; Giardina et al., 2010; Losacco et al., 2014) and the building weight (Burd et al., 2000; Liu et al., 2000; Franzius et al., 2004; Rampello et al., 2012; Giardina et al., 2015a). These aspects have been evaluated by using physical (Farrell, 2010; Laefer et al., 2011; Giardina et al., 2012; Nghiem et al., 2014) and numerical (Potts and Addenbrooke, 1997; Burd et al., 2000; Liu et al., 2000; Son and Cording, 2005, 2007; Boonpichetvong and Rots, 2005; Franzius et al., 2006; DeJong et al., 2008; Giardina et al., 2010; Pickhaver et al., 2010; Giardina et al., 2013; Amorosi et al., 2014; Losacco et al., 2014) models.

However, fewer numerical modelling studies have been validated with experimental results (Son and Cording, 2005; Giardina et al., 2013); in particular, computational modelling of the soil–structure interaction due to tunnelling-induced

* Corresponding author.
E-mail address: gg376@eng.cam.ac.uk (G. Giardina).

http://dx.doi.org/10.1016/j.tust.2015.07.016
0886-7798/

settlements has never been compared with centrifuge tests, which can reproduce the real stress conditions of the prototype due to the increased acceleration applied to scaled models. Centrifuge experiments have been recently performed on building models (metallic plates) of different weight and stiffness subject to tunnelling (Farrell, 2010). The results demonstrate that the soil–structure interaction may include the development of a gap between the structure and the soil. The occurrence and magnitude of the gap depends on the type of structure (particularly its stiffness and weight) and the amount of tunnelling induced ground settlement. These tests suggest that accurate simulation of the building response depends on the inclusion of the building weight and a no-tension soil–structure interface.

The effect of building weight has been numerically analysed (Franzius, 2003) under the assumption that for realistic values of weight and ground loss, no gap can develop between the soil and the building. The effect of the building weight was found to be negligible with respect to the effect of the relative stiffness. A no-tension interface between the structure and the soil has also been considered previously (Rots, 2000) to reduce the effect of a greenfield settlement profile directly applied to the structure; nonlinear interface elements between the soil and the structure have been used in subsequent numerical studies on building response to differential settlements (e.g. Boonpichetvong and Rots, 2005; Netzel, 2009; Giardina et al., 2013).

The aim of this study is to investigate the key aspects of modelling the interaction between tunnelling in sand and surface structures and to evaluate the effect of building weight on this interaction. A 2D finite element model with nonlinear interface elements is used to identify important modelling aspects, like the simulation of the experimentally observed soil–structure gap. The model is evaluated through comparison with centrifuge experiments by Farrell Farrell and Mair (2011). The model is then used to perform a sensitivity study on the interaction between the building stiffness and weight, the latter of which is typically neglected in the current damage assessment procedures.

2. Numerical model

Fig. 1a illustrates the experimental setup described by Farrell (2010) and reproduced by the numerical model presented in this paper (Fig. 1b). In the centrifuge experiment, a tunnel excavation was simulated under plane strain conditions in a high resistant steel box containing fine dry sand. The model was subjected to an acceleration of 75 g and therefore reproduced the response of a prototype 75 times larger. The volume loss induced by the tunnelling and the consequent settlements on the soil surface were obtained by gradually withdrawing water from a rubber membrane installed around the tunnel; the membrane pressure was steadily increased during the centrifuge spin-up so that it was always equal to the total vertical pressure at the tunnel axis. Having reached 75 g water was then gradually withdrawn from the membrane, simulating tunnel volume loss. After a preliminary test performed in greenfield conditions, four aluminium beams of different stiffness and weight were added to the model surface (Fig. 2), to investigate the soil–structure interaction induced by tunnelling.

To reproduce the boundary conditions imposed by the strong box, the vertical free edges of the numerical model were constrained in the horizontal direction, while the bottom side was fixed in both the vertical and horizontal direction (Fig. 1b). The centrifuge spin-up was simulated by incrementally increasing the gravity load up to 75 g. During this phase the tunnel was neglected. After the gravity load of 75 g was applied, the soil elements corresponding to the tunnel section were deactivated. In order to maintain equilibrium between internal and external forces, an outward radial pressure was simultaneously applied at the tunnel boundary. The surface settlement profile was obtained by gradually reducing the pressure up to zero and then by incrementally applying an inward radial pressure. The change of pressure was proportional to the initial equilibrium value.

Fig. 2 shows the mesh of the finite element model. Quadratic plane strain elements were used for the soil, the tunnel and the structures. The aluminium beams were modelled with an isotropic linear elastic material. Quadratic interface elements with no tensile strength, high stiffness in compression and low stiffness in shear were inserted between the soil and the structure. The compressive and shear behaviour of the interface was assumed to be linear elastic. All material parameters are listed in Table 1.

Two alternative constitutive laws were considered for the soil. Firstly, a linear relationship between the Young's modulus E and the depth z was assumed:

$$E(z) = E_0 + (z - z_0)\frac{\partial E}{\partial z} \tag{1}$$

where E_0 is the Young's modulus at the soil surface, z is the vertical coordinate of the soil, z_0 is the vertical coordinate of the soil surface and $\frac{\partial E}{\partial z}$ is the gradient of the Young's modulus in the vertical direction. Secondly, the isotropic strain invariant ε_v and the shear strain invariant ε_s were assumed to be dependent on the total mean normal stress p and the deviatoric stress q according to the following power-law relationship for undrained conditions:

$$\begin{cases} \varepsilon_v = \frac{1}{K_1}\left(\frac{p}{p_0}\right)^{n-1}\left(1 - \beta\frac{q^2}{p^2}\right)p \\ \varepsilon_s = \frac{1}{3G_1}\left(\frac{p}{p_0}\right)^{n-1} q \end{cases} \tag{2}$$

where K_1 is the reference compression modulus, G_1 is the reference shear modulus, n is a constant coefficient, p_0 is the reference pressure, equal to -1 kPa, and $\beta = \frac{K_1(1-n)}{6G_1}$. The values of K_1, G_1 and n are experimentally calibrated, as noted below. The Young's modulus is derived as $E = 2(1+\nu)G_1$, where $\nu = \frac{3K_1 - 2G_1}{6K_1 + 2G_1}$ is the Poisson's

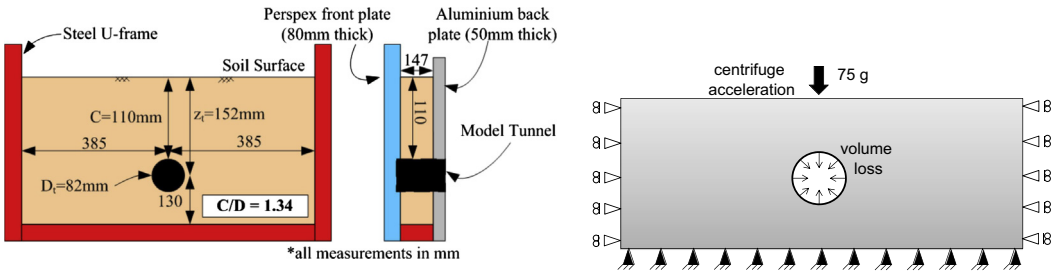

(a) experimental (Farrell, 2010) (b) numerical

Fig. 1. Greenfield model (dimensions in mm).

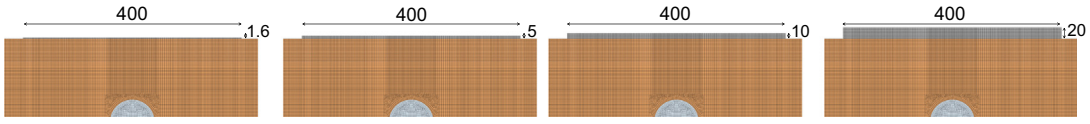

(a) STR-1 (b) STR-2 (c) STR-3 (d) STR-4

Fig. 2. Numerical model with structures (dimensions in mm).

Table 1
Material parameters for the numerical model.

Aluminium	Young's modulus	$E_a = 70 \times 10^3$ N/mm^2
	Density	$\rho_a = 2.7 \times 10^{-6}$ kg/mm^3
	Poisson's ratio	$\nu_a = 0.3$
Interface	Normal stiffness	$k_n = 100$ N/mm^3
	Tangent stiffness	$k_t = 0.1$ N/mm^3
	Tensile strength	$f_{t,b} = 0$ N/mm^2
Soil	Reference Young's modulus	$E_0 = 25$ N/mm^2
	Young's modulus gradient	$\frac{\partial E}{\partial z} = -4.5 \times 10^{-2}$ N/mm^3
	Density	$\rho_m = 1.59 \times 10^{-6}$ kg/mm^3
	Poisson's ratio	$\nu_m = 0.25$
	Reference shear modulus	$G_1 = 1$ N/mm^2
	Reference compression modulus	$K_1 = 2.5$ N/mm^2
	Power constant	$n = 0.53$
	Reference pressure	$p_0 = -1 \times 10^{-3}$ N/mm^2

ratio. The adopted soil models are evaluated based on their ability to reproduce the experimentally observed tunnelling-induced settlement profile at the surface level.

Fig. 3a shows the settlement of the soil above the tunnel centreline measured at the surface ($z = 0$) and at 60 mm below the surface ($z = 60$) during the spin-up of the centrifuge model from 0 to 75 g. These results are used to calibrate the values of the Young's modulus gradient $\frac{\partial E}{\partial z}$ of the linear elastic soil model and the values of n, K_1 and G_1 of the nonlinear elastic soil models. The comparison with the numerical results (Fig. 3b) indicates that the nonlinear elasticity provides a considerably better fit to the experimental curves, being capable of capturing the increase of soil stiffness with the increasing confining stress.

3. Simulation of centrifuge tests

In this section, the experimental results by Farrell (2010) are used to evaluate the numerical models. In particular, the comparison between experimental and numerical results is used to select the more adequate soil model, evaluate the need for using a no-tension interface between the soil and the structure and assess the model's ability to simulate the structural response.

3.1. Greenfield tests

Fig. 4 illustrates the results of the analysis in terms of surface settlements of the soil for increasing values of volume loss V_L; 'greenfield' conditions are assumed, i.e. no building is modelled. To compare the experimental and numerical results, the maximum vertical settlement for each value of V_L is assumed as reference. The nonlinear elastic model provides a better fit of the experimental curves, producing a settlement trough narrower than the one predicted by the linear elastic model. Since damage to buildings is proportional to the angular distortion imposed by the settlement trough (Skempton and MacDonald, 1956), accurate modelling of the trough shape and width is important for the evaluation of soil-interaction effects. The nonlinear elastic soil model has been therefore selected to perform the subsequent analyses.

Particle Image Velocimetry (PIV) measurements of the greenfield vertical and horizontal displacements of the soil (Fig. 5a) were also used to evaluate the performance of the selected soil model. Although the simplified assumption of neglecting a failure criterion for the soil does not allow the model to capture the failure mechanism propagating up from the tunnel crown at high volume losses (Fig. 5a), the model is able to simulate the gradual decrease of settlement towards the ground surface. Also the distribution of horizontal settlements within the soil is adequately simulated by the computational model (Fig. 6). The model does reproduce the experimental concentration of the displacements between the tunnel shoulders and the soil surface for increasing volume loss, with larger displacements at the tunnel shoulders and soil surface and negligible displacements above the tunnel centreline. Note that at volume loss $V_L = 0.5\%$ the displacements measured experimentally were close to the limit precision of PIV (0.01 mm (Farrell, 2010)), making the top pair of figures in Fig. 6 less suitable for direct comparison.

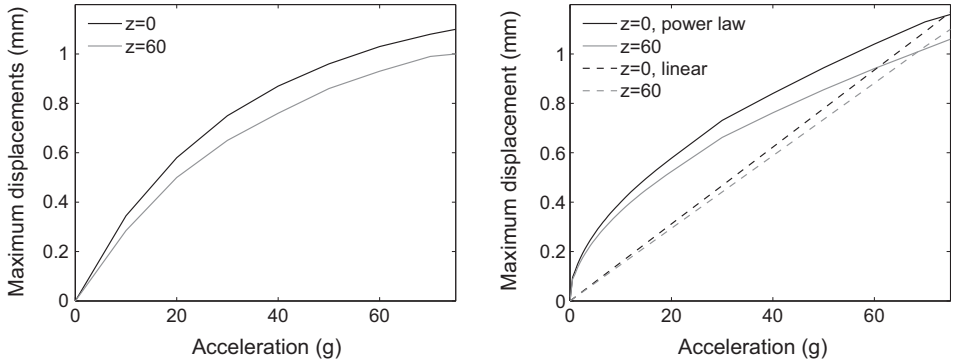

(a) experimental (Farrell, 2010) (b) numerical

Fig. 3. Maximum settlement above the tunnel during centrifuge spin-up.

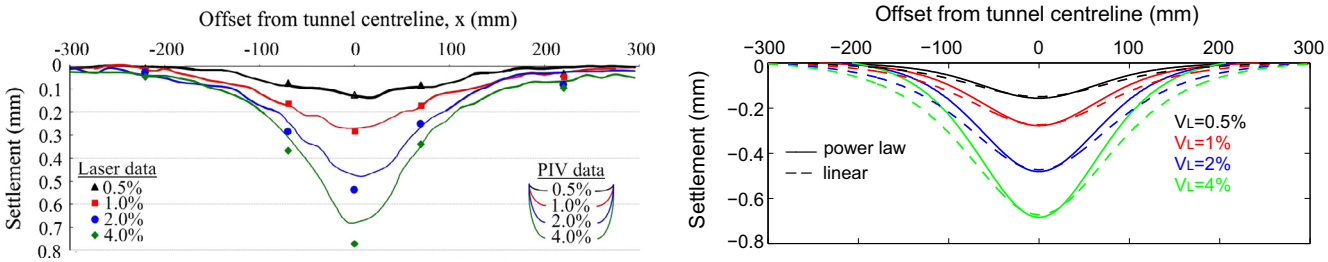

(a) experimental (Farrell, 2010) (b) numerical

Fig. 4. Greenfield vertical displacements of the soil surface.

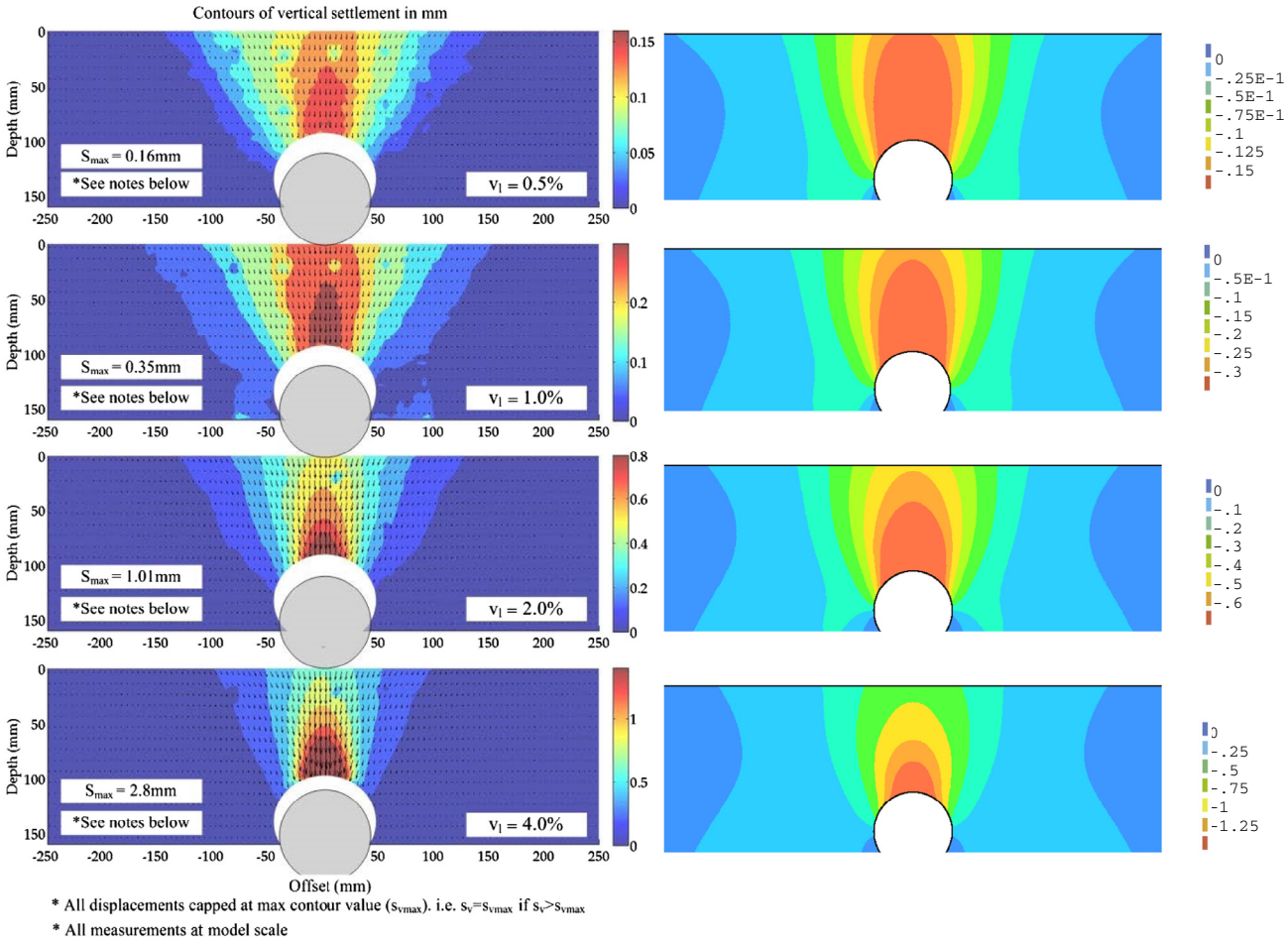

(a) experimental (Farrell, 2010) (b) numerical

Fig. 5. Contour plot of soil vertical displacements, greenfield case.

3.2. Soil–structure interaction tests

Fig. 7 compares the experimental and numerical displacements of the most flexible (STR-1) and stiffest (STR-4) beams in the vertical direction. The numerical curves, labelled with increasing volume losses to facilitate the visual comparison, correspond to the same values of tunnel radial pressure which produced the greenfield curves in Fig. 4b (also shown in Fig. 7a). The numerical model correctly reproduces both the behaviour of the flexible beam, which follows closely the greenfield deformations, and the stiff beam, which exhibits a significantly smaller deflection. The vertical displacement of the soil surface is shown in Fig. 8. Figs. 2a and 8a show a significant difference between the vertical displacements of STR-4 and the settlements of the soil beneath the structure; this difference could not be explained without taking into account the formation of a gap between the soil and the structure base. The key element for an accurate prediction of the experimental results is therefore the use of a no-tension interface between the soil and the beam. Fig. 7b shows that without the interface the structure would be pulled by the subsiding soil, reaching a final deformation of intermediate magnitude between the experimental test and the greenfield case. This interpretation is supported by the experimental measurements of the soil–structure gap (Fig. 9a). The model with the interface captures the increase of the gap as the beam stiffness and the volume loss increase, and provides a good prediction of the gap values for all the analysed structures (Fig. 9b).

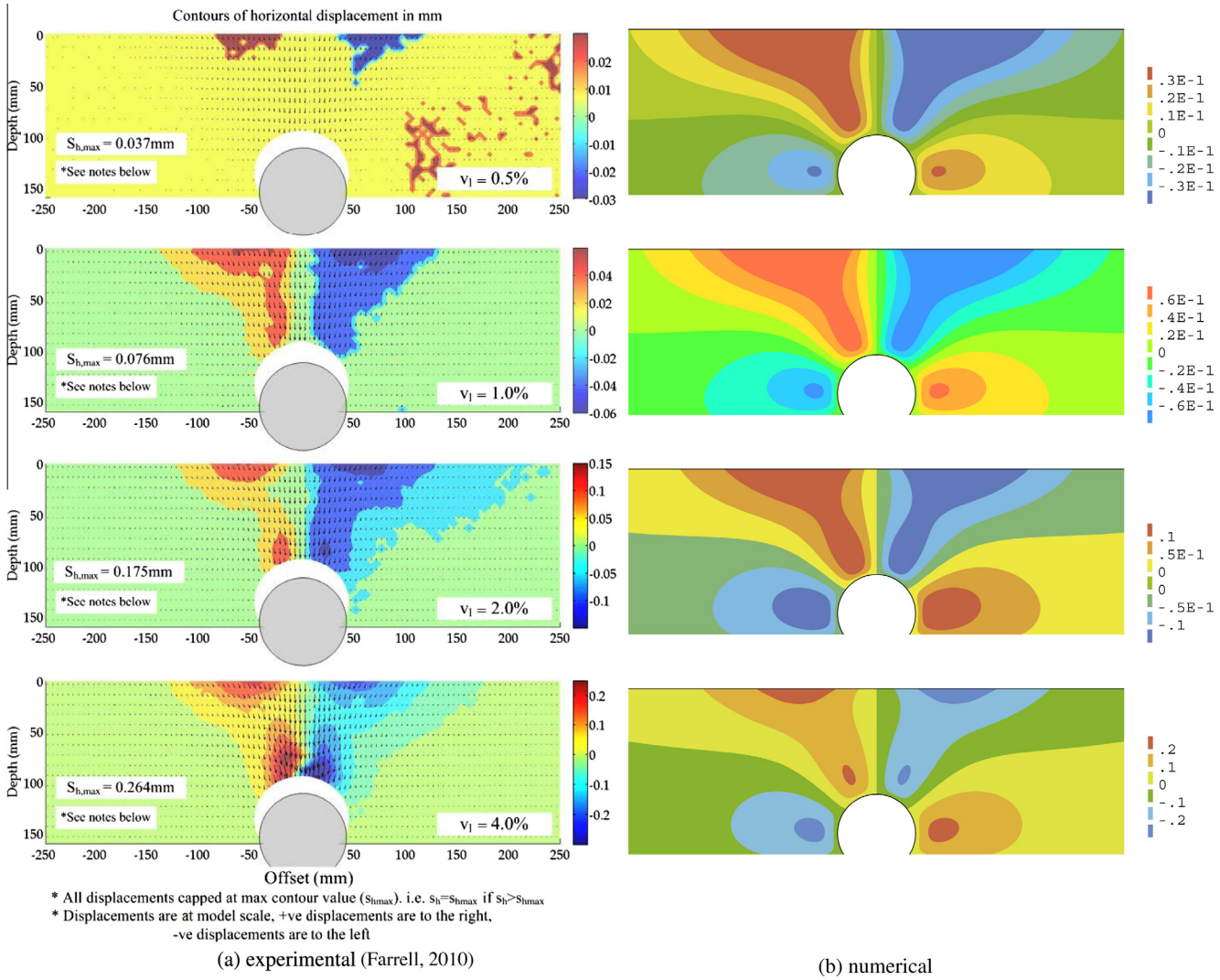

(a) experimental (Farrell, 2010) (b) numerical

Fig. 6. Contour plot of soil horizontal displacements, greenfield case.

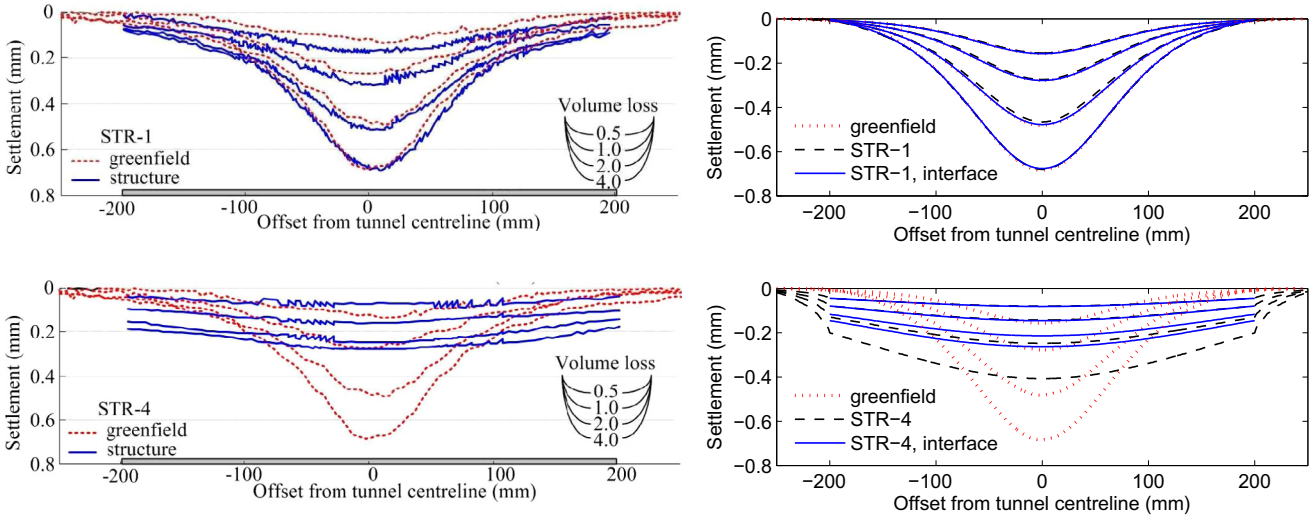

(a) experimental (Farrell, 2010) (b) numerical

Fig. 7. Vertical displacements of aluminium beam structures.

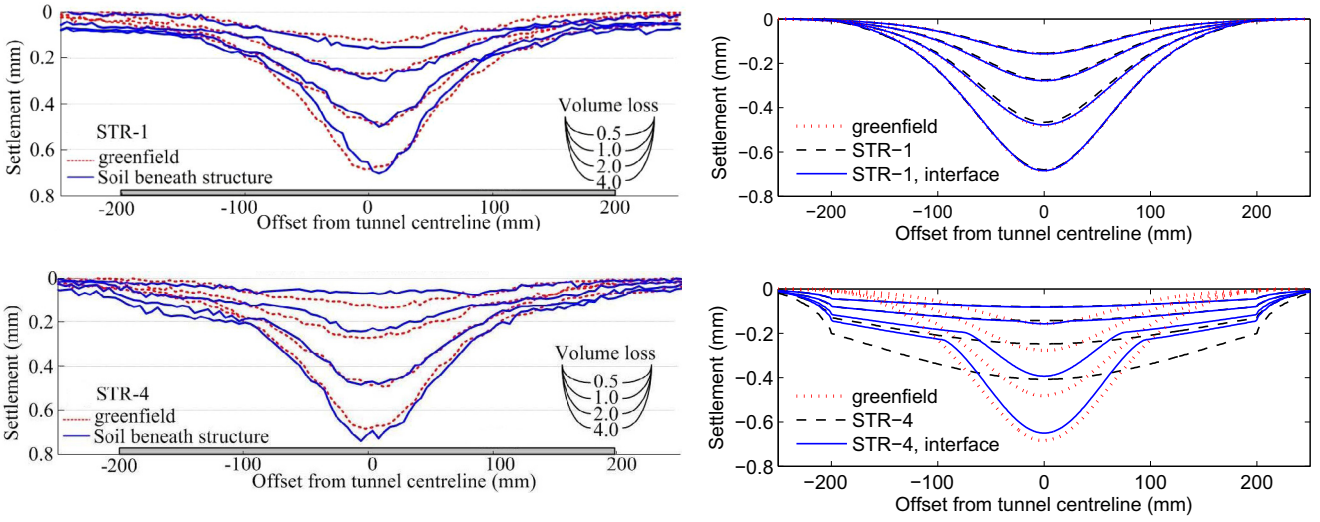

(a) experimental (Farrell, 2010) (b) numerical

Fig. 8. Vertical displacements of soil.

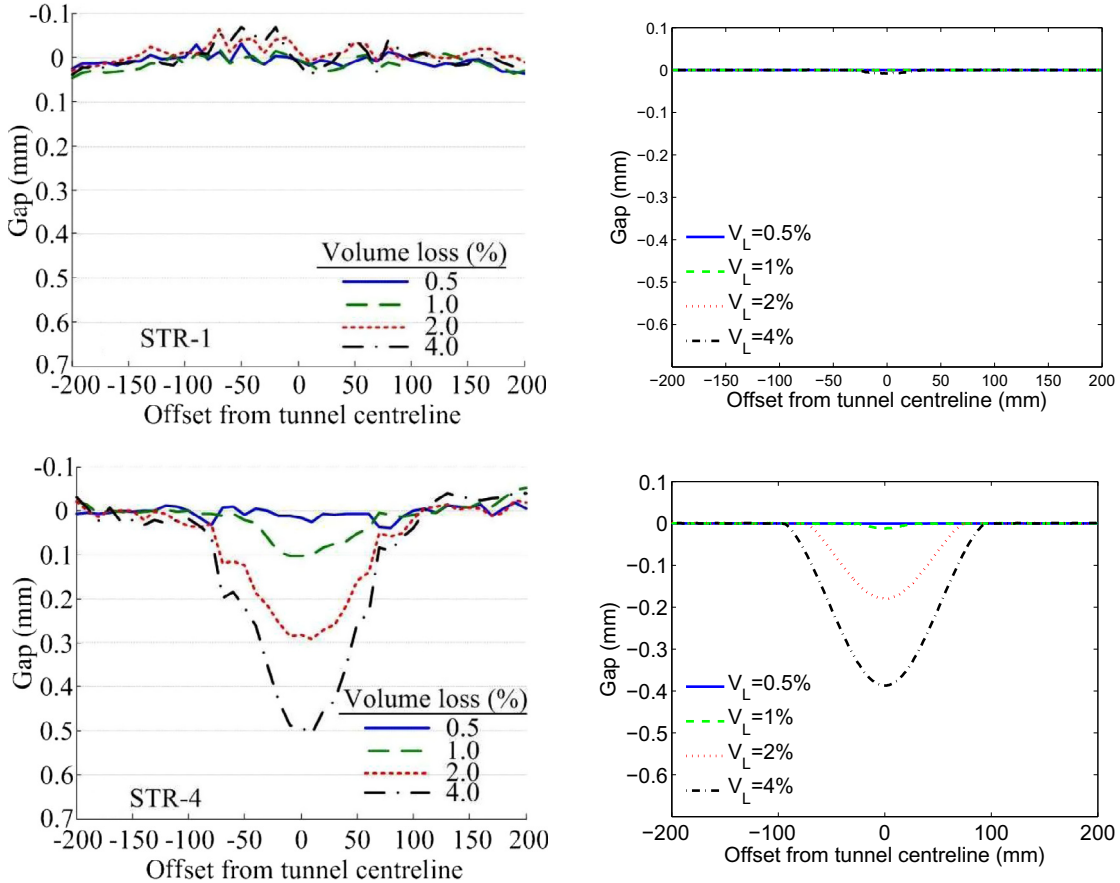

(a) experimental (Farrell, 2010) (b) numerical

Fig. 9. Soil–structure gap.

Horizontal displacements of the beam and soil surface are presented in Figs. 10 and 11. Consistent with field data (Mair, 2003), the structures do not develop significant horizontal displacements (Fig. 10), and therefore negligible horizontal strains arise. Furthermore, the structures act as a partial restraint to the soil, which exhibits horizontal displacements either smaller than or equal to the greenfield case (Fig. 11). As for the vertical displacements of the beam, the response of the soil in the horizontal direction is connected with the soil–structure gap. For STR-4 and higher values of volume loss, the soil–structure gap allows the maximum

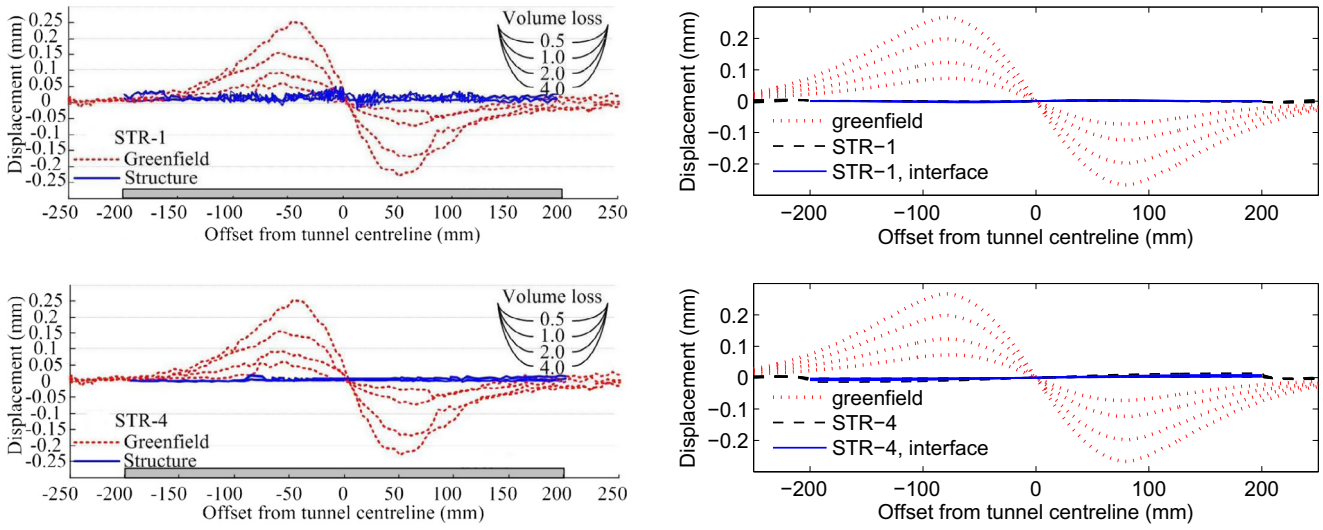

(a) experimental (Farrell, 2010) (b) numerical

Fig. 10. Horizontal displacements of aluminium beam structures.

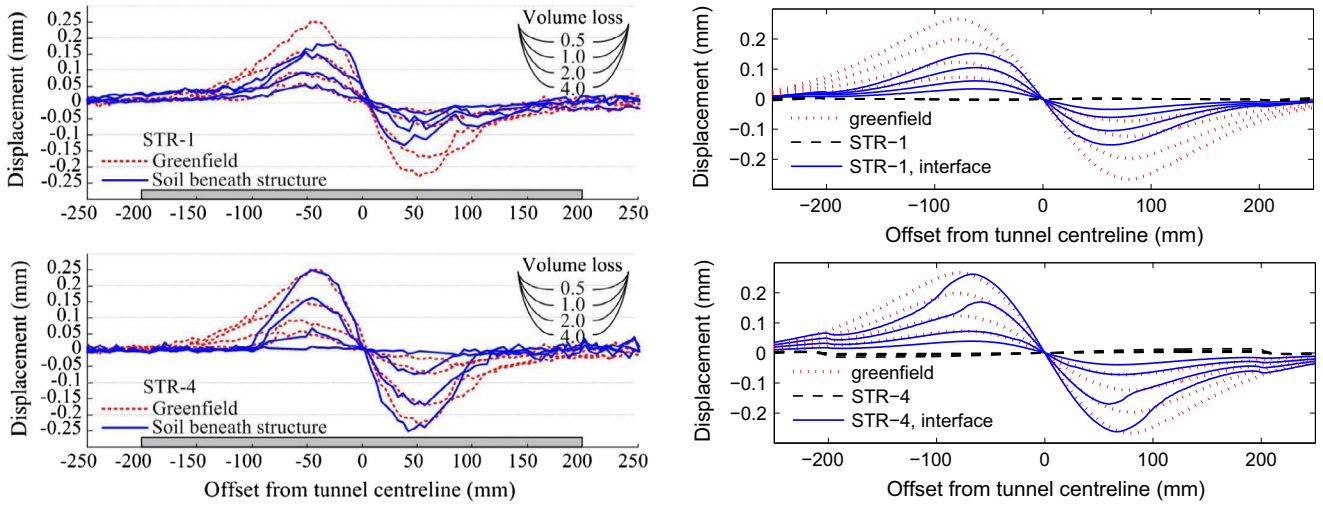

(a) experimental (Farrell, 2010) (b) numerical

Fig. 11. Horizontal displacements of soil.

soil displacements to nearly match the greenfield results. However, at greater distances from the tunnel centreline, the gap closes and the horizontal soil displacements are negligible (Fig. 11a). For all volume losses and structures the numerical model produces profiles in reasonable agreement with the experimental curves, with a general tendency to overestimate the displacements close to the area of the beam where the gap is formed.

The analyses of the soil vertical displacements with and without surface structures (Fig. 12) confirm the capability of the model to reproduce the increase in settlement trough width due to the presence of the aluminium beam. The effect is particularly evident when comparing the greenfield case with the STR-4 results (first and fourth rows of Fig. 12, respectively).

As mentioned in Section 3.1, the nonlinear elastic model captures the surface displacements with acceptable accuracy up to realistic values of volume loss, after which the failure mechanism propagating from the tunnel crown would govern the settlement profile. Similarly, the model captures the interaction between the soil and surface structures on shallow foundations, but effective modelling of buildings on pile foundations would likely require inclusion of a soil failure mechanism. Additionally, the linear elastic assumption is appropriate for aluminium beams and for identifying when cracking will occur, but modelling the post-cracking response of an existing structure would require a nonlinear material model.

3.3. Modification factors

In an extension of the assessment method by Burland and Wroth (1974), based on the concept of critical strain, Potts and

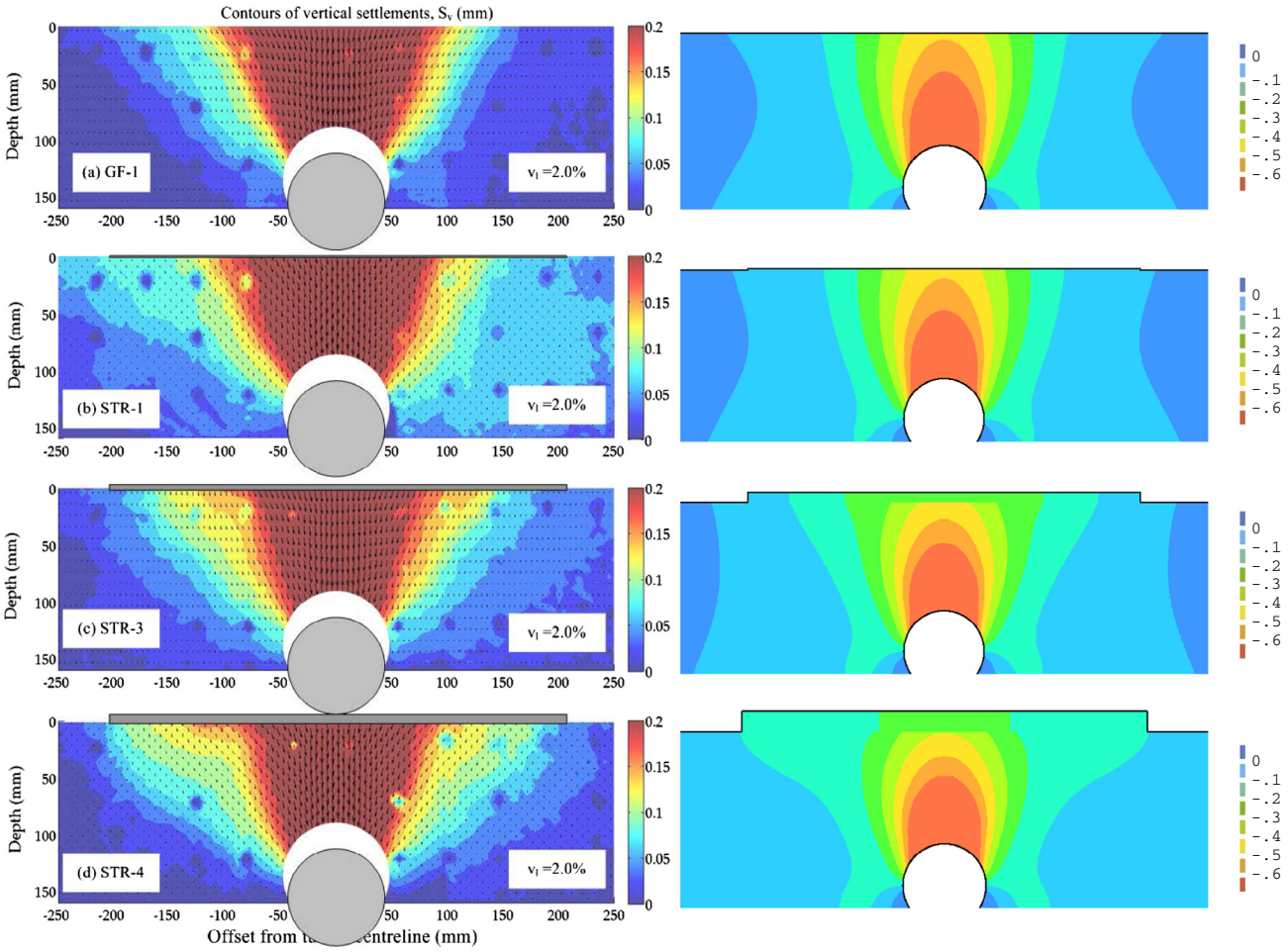

Fig. 12. Contour plot of soil vertical displacements. From top to bottom: greenfield case, STR-1, STR-3 and STR-4.

Addenbrooke (1997) measured the effect of the soil–structure interaction on the beam deflection by using the modification factors:

$$M_{DR,\mathrm{sag}} = \frac{(\Delta_{\mathrm{sag}}/L_{\mathrm{sag}})}{(\Delta_{\mathrm{sag}}/L_{\mathrm{sag}})_{gr}} \quad M_{DR,\mathrm{hog}} = \frac{(\Delta_{\mathrm{hog}}/L_{\mathrm{hog}})}{(\Delta_{\mathrm{hog}}/L_{\mathrm{hog}})_{gr}} \tag{3}$$

where L_{sag} and L_{hog} are the building length in the concave (sagging) and convex (hogging) part of the greenfield settlement profile, respectively, $\Delta_{\mathrm{sag}}/L_{\mathrm{sag}}$ and $\Delta_{\mathrm{hog}}/L_{\mathrm{hog}}$ are the corresponding ratios between the relative deflection Δ, defined as the maximum displacement relative to the straight line connecting the two ends of the sagging and hogging part of the building base, and the respective building length, while $(\Delta_{\mathrm{sag}}/L_{\mathrm{sag}})_{gr}$ and $(\Delta_{\mathrm{hog}}/L_{\mathrm{hog}})_{gr}$ are the greenfield deflection ratios that would occur without the structure. Potts and Addenbrooke proposed design charts to associate the modification factor to specific features of the building and the soil, summarised in the relative bending stiffness:

$$\rho^* = \frac{EI}{E_s(L/2)^4} \tag{4}$$

where E is the Young's modulus, I is the second moment of area of the cross section, L is the total building length and E_s is the soil characteristic stiffness. Franzius et al. (2006) modified the relative stiffness, which was originally defined in plane strain conditions, to make it dimensionless in both two and three dimensions, by including the effect of the tunnel depth z_0 and the building width B:

$$\rho^*_{\mathrm{mod}} = \frac{EI}{E_s L^2 z_0 B} \tag{5}$$

Based on experimental tests and field data, Farrell (2010) partitioned the relative bending stiffness in the sagging and hogging zone of the greenfield settlement profile curvature:

$$\rho^*_{\mathrm{sag,par}} = \frac{EI}{E_s L^3_{\mathrm{sag}} B} \quad \rho^*_{\mathrm{hog,par}} = \frac{EI}{E_s L^3_{\mathrm{hog}} B} \tag{6}$$

The modification factor for the deflection ratio has been used to complete the validation of the numerical model in terms of global structural deformation. Fig. 13 shows the modification factors versus the relative bending stiffness as defined in Eq. (5), while Fig. 14 shows the same but for the relative bending stiffness values defined by Eq. (6). Note that in the experimental graph the soil stiffness is assumed to be dependent on the volume loss and therefore the relative stiffness increases for increasing values of volume loss (Farrell, 2010). In the numerical model, a single reference value for the soil stiffness is assumed throughout the whole analysis. For each structure, the numerical results show a range of modification factors comparable to the experimental values.

For small values of relative stiffness, the structure deformations are generally similar to the greenfield ones and therefore the modification factor M_{DR} is close to unity, while for increasing values of relative stiffness the beam deflection ratio reduces and so does M_{DR}. With respect to the experimental results, the numerical

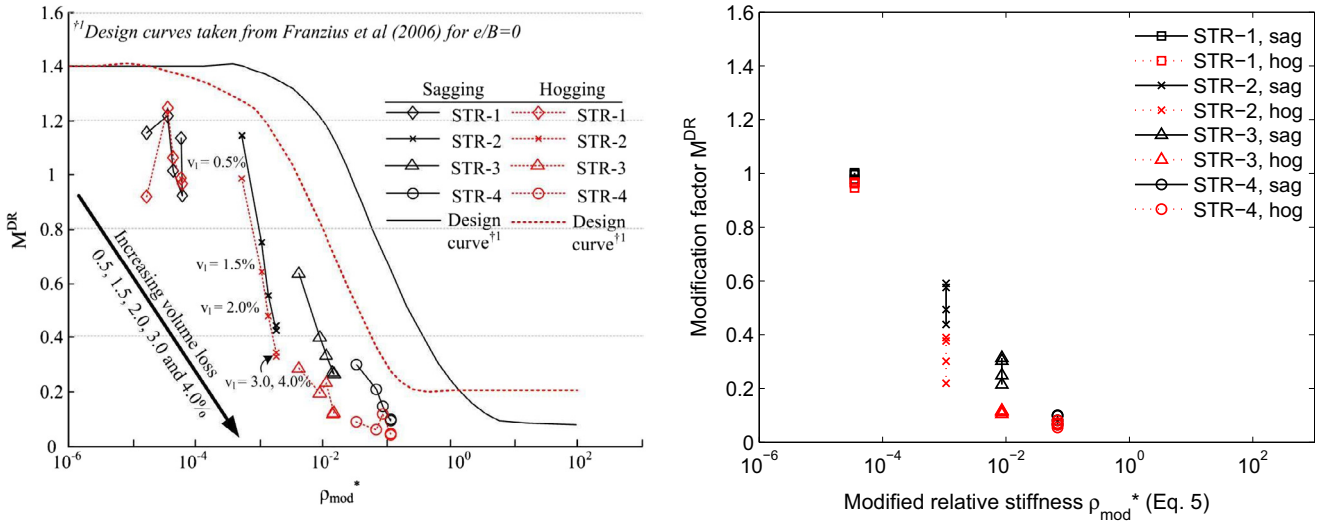

(a) experimental (Farrell, 2010) (b) numerical

Fig. 13. Deflection ratio modification factor vs modified relative bending stiffness (Eq. (5)).

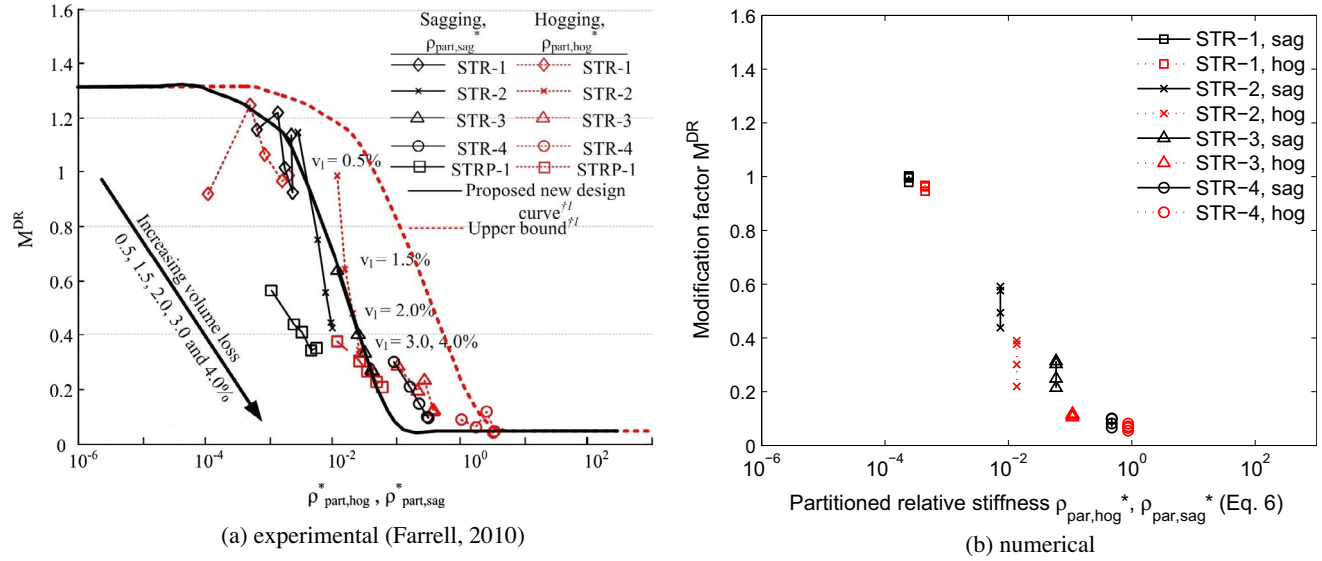

(a) experimental (Farrell, 2010) (b) numerical

Fig. 14. Deflection ratio modification factor vs partitioned modified relative bending stiffness (Eq. (6)).

model tends to underestimate the modification factors for the most flexible structure and for the lowest value of volume loss. These are the cases where the beam distortion approximates to the greenfield one, sometimes showing displacements even larger than in the greenfield case (Fig. 7a, STR-1). The main reason for this is the embedding of the ends of the structure into the soil, a mechanism which is not captured by the numerical model. However, the results provide a generally good estimation of the modification factors over a wide range of structure stiffness. This offers a reliable base to perform a sensitivity study on how the building weight influences the soil–structure interaction mechanism.

4. Effect of building weight

The results above indicates the presence of a gap between the soil and the structure in the case of stiffer structures and higher volume loss values. This section investigates how that gap, and the soil–structure interaction more generally, may be affected by the weight of the structure, which is typically ignored in assessment procedures. The building stiffness and weight variations selected are first presented, followed by the results of the parametric study. Differences with results from previous studies are highlighted and discussed.

4.1. Parametric variations

Fig. 15a gives a graphical overview of the numerically tested structures in terms of bending and axial stiffness at prototype scale. The variations include structures STR-1 to STR-4 from Section 3, as well as new structures STR-5 to STR-8. In order to relate these variations to real buildings, data from buildings monitored during the Jubilee Line Extension (Mair and Taylor, 2001; Dimmock and Mair, 2008) are also shown in the graph. The selected stiffness values represent an upper and lower envelope for the real stiffnesses, particularly for the bending stiffness when calculated with the methodologies described in Mair and Taylor (2001) and Dimmock and Mair (2008). The exact stiffness values assumed in the parametric study are reported in Table 2.

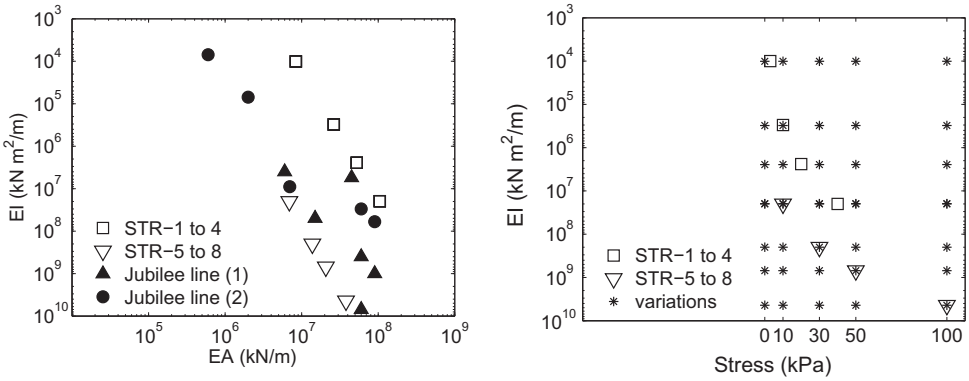

(a) Bending (EI) vs axial (EA) stiffness for numerical variations and field data

(1) EI and EA according to Mair and Taylor (2001)

(2) EI and EA according to Dimmock and Mair (2008)

(b) Base stress vs bending stiffness for numerical variations

Fig. 15. Bending stiffness, axial stiffness and base stress at the prototype scale for the reference centrifuge models, real buildings and the parametric variations performed in this study.

Table 2
Parametric variations of bending and axial stiffness combination.

	Axial stiffness *EA* (kN/m)	Bending stiffness *EI* (kN m)		Axial stiffness *EA* (kN/m)	Bending stiffness *EI* (kN m)
STR-1	8.4×10^6	1.0×10^4	STR-5	6.9×10^6	2.0×10^7
STR-2	2.6×10^7	3.0×10^5	STR-6	1.4×10^7	2.0×10^8
STR-3	5.2×10^7	2.4×10^6	STR-7	2.1×10^7	6.0×10^8
STR-4	1.0×10^8	2.0×10^7	STR-8	3.8×10^7	4.4×10^9

Table 3
Parametric variations of weight.

	Base stress (kN/m²)
σ_1	10
σ_2	30
σ_3	50
σ_4	100

Four different values of weight were applied to each of the analysed structures. These values approximate to the stresses acting at the base of real buildings of 1, 3, 5 and 10 storeys (Franzius et al., 2004) and they are listed in Table 3. Fig. 15b shows the complete set of variations in terms of bending stiffness and base stresses.

4.2. Results

Fig. 16 shows the effect of the weight on the deflection of STR-1 and STR-4 for selected volume losses. The results indicate that the vertical displacements of the beam increase with increasing applied weight. For higher volume losses this effect can be substantial: in the range of assumed weights, a significant loading can increase the beam settlements up to 70%. For relatively stiff structures, the weight influences the embedding of the structure into the soil, which is indicated by the vertical displacements at the two ends of the beam (Fig. 16d) and the development of the gap between the soil and the beam base in the case of the stiffer structure STR-4 (Fig. 17); Fig. 17 shows how the increase in weight tends to make the structure STR-4 follow the soil displacements and therefore reduces the gap.

The modification factors derived from the numerical analysis for all the structures, for a representative volume loss of 0.5% are plotted in Fig. 18a and b as a function of the partitioned relative stiffness in sagging and hogging, respectively (Eq. (6)). The results indicate that higher loading can lead to an increased modification factor, suggesting that the weight of the structure can reduce the effect of an increment in relative stiffness.

The impact of the weight on the building response is particularly significant when considering that this factor is neglected in the empirical–analytical procedures currently used for the assessment of potential damage. As introduced in Section 1, these procedures are based on the analyses performed on weightless beam models of buildings (Burland and Wroth, 1974; Potts and Addenbrooke, 1997). Later numerical analyses (Franzius et al., 2004) assessed the weight as a negligible factor if compared with the corresponding realistic variations of bending stiffness values. These analyses (Franzius et al., 2004), although including a comprehensive evaluation of variation of weight, consider a smaller range of relative stiffness values and were derived from a numerical model which neglected the possibility of a gap between the soil and the structure. The assumption of no gap was numerically evaluated by verifying the absence of normal tensile forces at the soil–beam interface for a singular case of stiffness and weight. While this check seems reasonable, the experimental data (Farrell, 2010) show that the structural response can involve the formation of a soil–structure gap. It should be noted that the values of relative stiffness and weight simulated by Farrell (2010) are within the realistic range of values for existing buildings. In addition, the numerical analyses described in this paper, characterised by the specific simulation of the soil-interface gap, suggest the relevance of the weight in the experimentally observed mechanism by including a wider range of stiffness values. The need to include the building weight in 2D and 3D numerical modelling of tunnelling has also been stated by Liu et al. (2000) and Rampello et al. (2012), respectively.

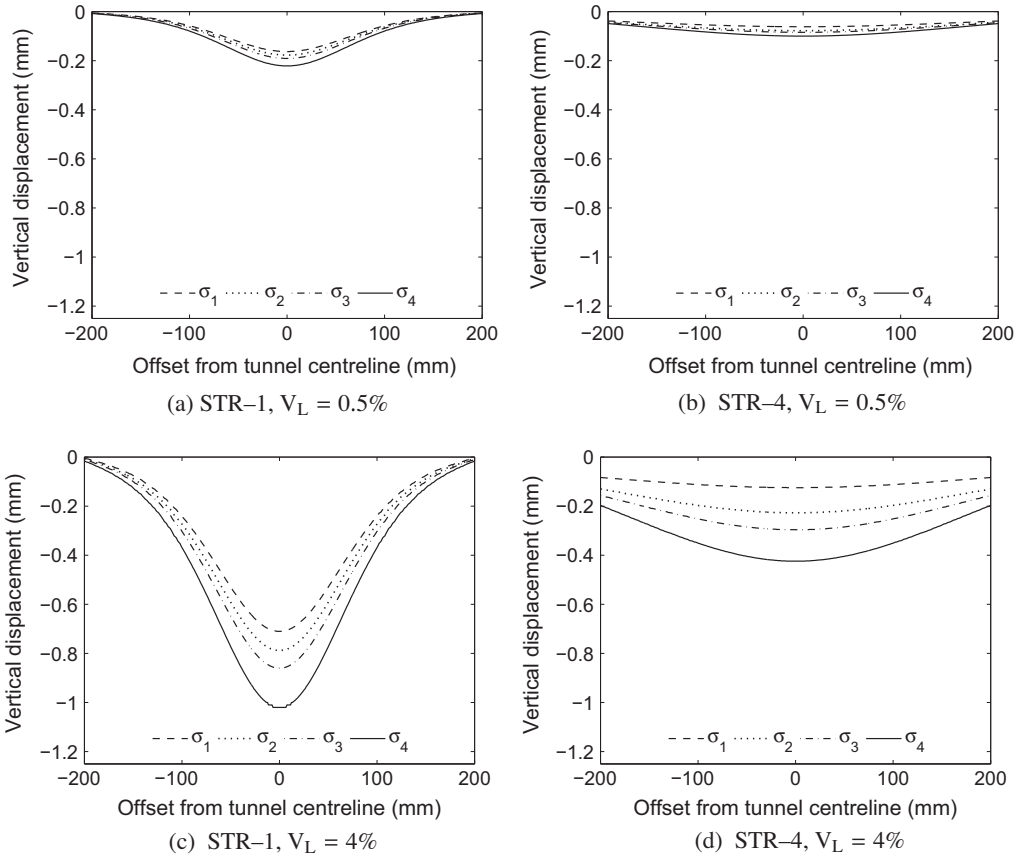

(a) STR–1, $V_L = 0.5\%$ (b) STR–4, $V_L = 0.5\%$

(c) STR–1, $V_L = 4\%$ (d) STR–4, $V_L = 4\%$

Fig. 16. Weight influence on the vertical displacements of selected structures (STR-1 and STR-4).

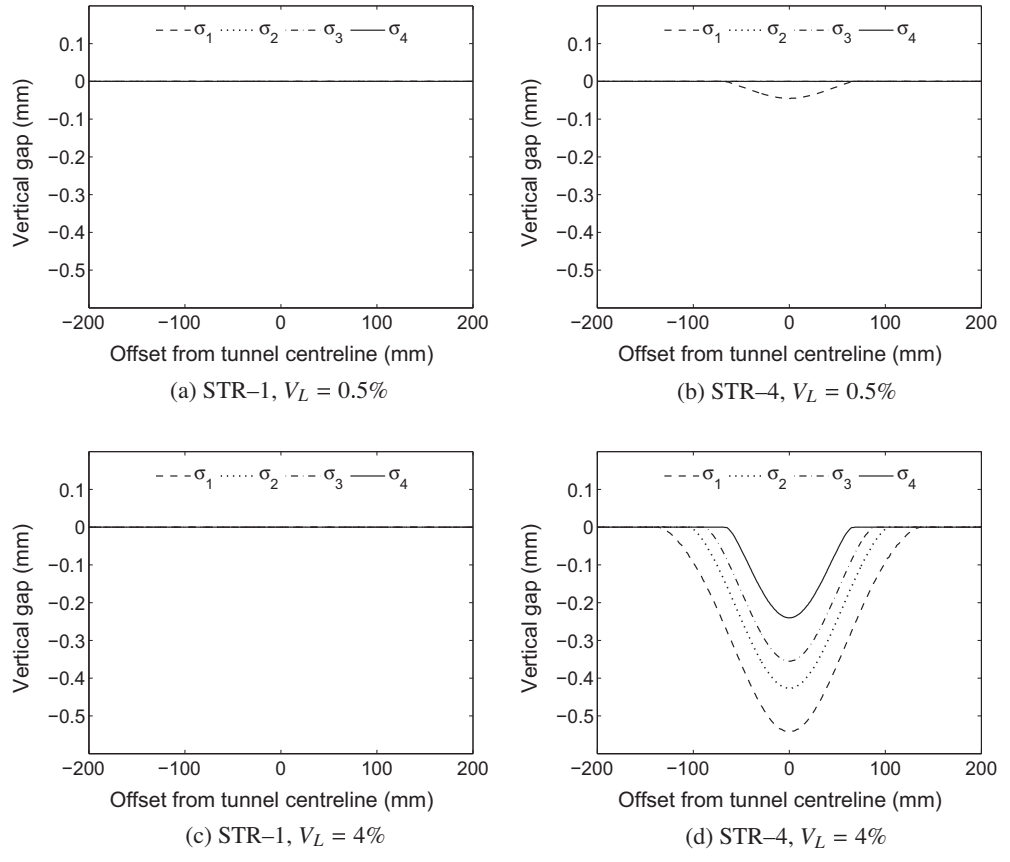

(a) STR–1, $V_L = 0.5\%$ (b) STR–4, $V_L = 0.5\%$

(c) STR–1, $V_L = 4\%$ (d) STR–4, $V_L = 4\%$

Fig. 17. Weight influence on the gap between the soil and selected structures (STR-1 and STR-4).

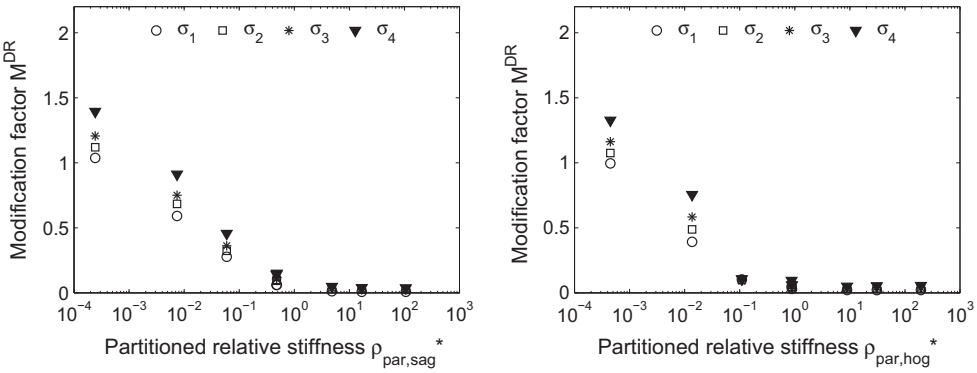

(a) $V_L = 0.5\%$, sagging (b) $V_L = 0.5\%$, hogging

Fig. 18. Deflection ratio modification factor vs relative bending stiffness (Eq. (6)), all variations.

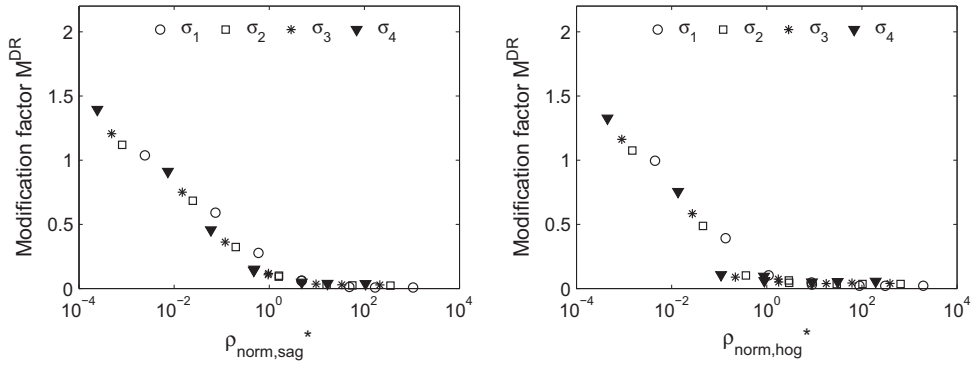

(a) $V_L = 0.5\%$, sagging (b) $V_L = 0.5\%$, hogging

Fig. 19. Deflection ratio modification factor vs normalised relative bending stiffness, all variations.

Fig. 18 highlights that the impact of the building weight on the modification factor decreases with the increase in relative stiffness. This suggests a possibility to correlate the modification factors with an indicator that combines the relative stiffness and weight of a structure. For example, a normalised relative stiffness ρ_{norm} can be defined in sagging and hogging as:

$$\rho_{norm,sag} = \frac{\rho^*_{sag,par}}{\frac{\sigma}{\sigma_1}} \quad \rho_{norm,hog} = \frac{\rho^*_{hog,par}}{\frac{\sigma}{\sigma_1}} \tag{7}$$

where σ is the total bearing pressure acting at the building foundations and σ_1 is the bearing pressure produced by one typical storey of the same building.

For cases where the building weight and bearing pressure are directly correlated with the number of storeys, like in this study (Table 2), the dimensionless coefficient $\frac{\sigma}{\sigma_1}$ corresponds to the number of storeys n_s:

$$\rho_{norm,sag} = \frac{\rho^*_{sag,par}}{n_s} \quad \rho_{norm,hog} = \frac{\rho^*_{hog,par}}{n_s} \tag{8}$$

In Fig. 19, the modification factors are shown as a function of ρ_{norm}, again for a volume loss of 0.5%. The modification factors tend to align, identifying a decrease with the increase of the normalised relative stiffness. Similar results were found for higher values of V_L. In Fig. 20, the numerical results in terms of modification factors are plotted first against the partitioned relative stiffness (Eq. (6)) and then against the normalised relative stiffness (Eq. (8)) for all values of volume loss.

When the weight is included in the building characterisation, the results fall into a narrower band within the envelope identified by Mair (2013) which applies to centrifuge models and field case histories. For values of $\rho^*_{par} < 10^{-4}$ and $\rho^*_{par} > 1$, the structure behaves as fully flexible and fully rigidly, respectively. For this reason, only the numerical results corresponding to $10^{-4} < \rho^*_{par} < 1$ are included in Fig. 20a and b. The analysis of the centrifuge data from Farrell (2010) (Fig. 20c) and the numerical results from Potts and Addenbrooke (1997) (Fig. 20d) is consistent with this. It should be noted that the weight effect is included only for structures with weight corresponding to one or more storeys. The coefficient n_s in Eq. (8) is assumed equal to 1 in the other cases. For the weightless beams analysed by Potts and Addenbrooke, the normalised stiffness therefore coincides with the relative stiffness.

5. Conclusions

In this paper, the interaction between tunnelling in sand and surface structures has been numerically investigated. A 2D finite element model with nonlinear interface elements was used to investigate the role of the soil–structure gap in modifying the soil greenfield settlement and building response. The comparison with the results of centrifuge tests showed that the model effectively reproduces the experimentally measured soil and structure displacements and that the use of a no-tension interface is necessary to simulate the soil–structure gap and the building deformation in the case of stiffer buildings.

The numerical model was then used to perform a sensitivity study on the interaction between building stiffness and weight. The results show that the building response depends not only on the relative stiffness between the structure and the soil but also

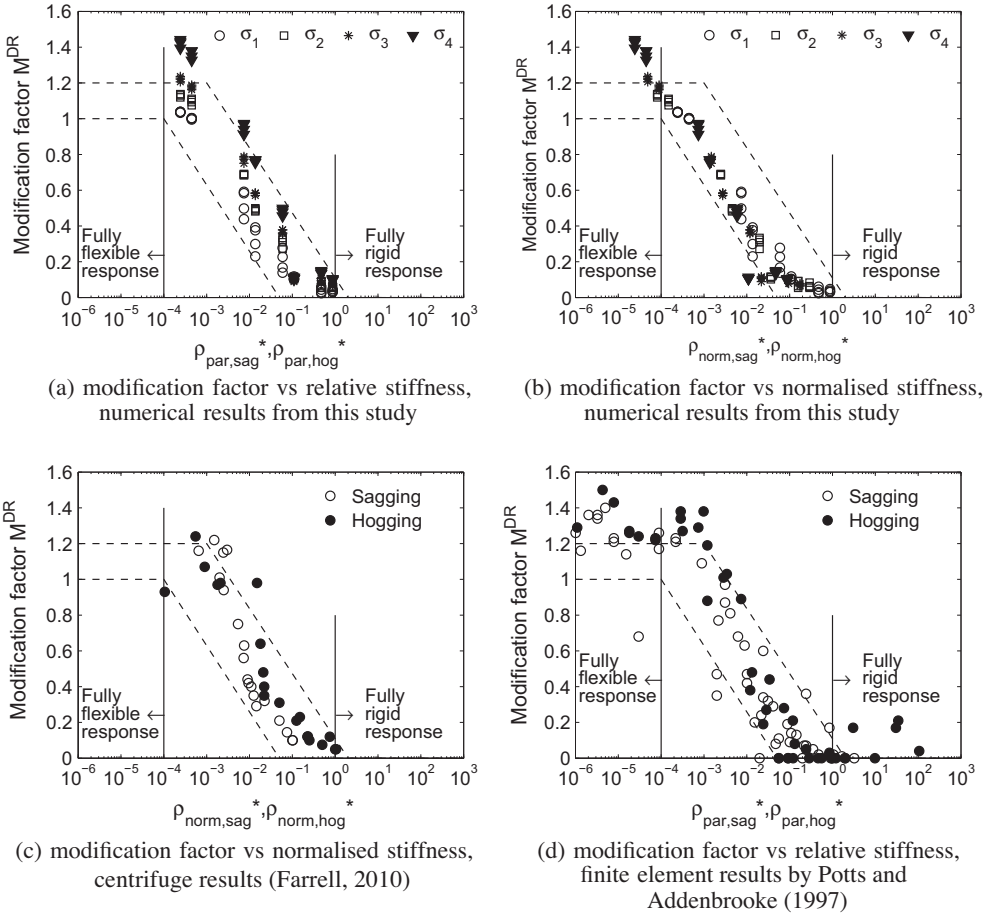

(a) modification factor vs relative stiffness, numerical results from this study

(b) modification factor vs normalised stiffness, numerical results from this study

(c) modification factor vs normalised stiffness, centrifuge results (Farrell, 2010)

(d) modification factor vs relative stiffness, finite element results by Potts and Addenbrooke (1997)

Fig. 20. Deflection ratio modification factor vs relative and normalised bending stiffness: comparison with centrifuge, numerical and field data. The dotted lines define the envelope identified by Mair (2013).

on the building weight, which is typically neglected in the current assessment procedures. The presentation of results in terms of relative stiffness normalised to a dimensionless indicator of the building weight demonstrated the potential value of including the weight in the damage assessment and was shown to be consistent with available experimental and numerical observations.

Acknowledgements

Financial support was provided by the Engineering and Physical Sciences Research Council of the United Kingdom, under Grant reference number EP/K018221/1. The research materials supporting this publication can be accessed at https://www.repository.cam.ac.uk/handle/1810/249085. The authors would like to acknowledge Dr. Ruaidhri Farrell for providing experimental data.

References

Amorosi, A., Boldini, D., De Felice, G., Malena, M., Sebastianelli, M., 2014. Tunnelling-induced deformation and damage on historical masonry structures. Geotechnique 64 (2), 118–130.

Boonpichetvong, M., Rots, J.G., 2005. Settlement damage of masonry buildings in soft-ground tunnelling. Struct. Eng. 83 (1), 32–37.

Boscardin, M.D., Cording, E.J., 1989. Building response to excavation-induced settlement. J. Geotech. Eng. 115 (1), 1–21.

BRE, 1995. Digest 251: Assessment of Damage in Low Rise Buildings with Particular Reference to Progressive Foundation Movements. Building Research Establishment, Tech. rep. Building Research Establishment.

Burd, H.J., Houlsby, G.T., Augarde, C.E., G, L., 2000. Modelling tunnelling-induced settlement of masonry buildings. Proc. Inst. Civil. Eng.: Geotech. Eng. 143 (1), 17–29.

Burland, J.B., 1995. Assessment of risk of damage to buildings due to tunneling and excavation. In: Ishihara, K. (Ed.), Proceedings of the 1st International Conference on Earthquake Geotechnical Engineering. A.A. Balkema, IS, Tokyo, Japan, pp. 1189–1201.

Burland, J.B., Wroth, C.P., 1974. Settlement of buildings and associated damage. In: Proceedings of Conference on Settlement of Structures. Pentech Press, Cambridge, pp. 611–654.

Burland, J.B., Broms, B.B., de Mello, V.F.B., 1977. Behaviour of foundations and structures. In: Proceedings of the 9th International Conference on Soil Mechanics and Foundation Engineering, vol. 2, 1977, pp. 495–546.

Clarke, J., Laefer, D.F., 2014. Evaluation of risk assessment procedures for buildings adjacent to tunnelling works. Tunnel. Under. Space Technol. 40, 333–342.

DeJong, M.J., Hendriks, M.A.N., Rots, J.G., 2008. Sequentially linear analysis of fracture under non-proportional loading. Eng. Fract. Mech. 75 (18), 5042–5056.

Devriendt, M., Palmer, E., Hill, R., Lazarus, D., 2013. Historic and non-historic building impact assessment methodology for major tunnelling infrastructure projects. In: Viggiani, C. (Ed.), Geotechnical Engineering for the Preservation of Monuments and Historic Sites. CRC Press, pp. 335–341.

Dimmock, P.S., Mair, R.J., 2008. Effect of building stiffness on tunnelling-induced ground movement. Tunnel. Under. Space Technol. 23, 438–450.

Farrell, R.P., 2010. Tunnelling in Sands and the Response of Buildings, Ph.D. thesis. University of Cambridge.

Farrell, R.P., Mair, R.J., 2011. Centrifuge modelling of the response of buildings to tunnelling. In: Seward, L. (Ed.), Physical Modelling in Geotechnics, Proceedings of the 7th International Conference on Physical Modelling in Geotechnics, Vol. 2. CRC Press, Zurich, Switzerland, pp. 549–554.

Franzius, J.N., 2003. Behaviour of Buildings Due to Tunnel Induced Subsidence, Ph.D. thesis. Imperial College, London.

Franzius, J.N., Potts, D.M., Addenbrooke, T.I., Burland, J.B., 2004. The influence of building weight on tunnelling-induced ground and building deformation. Soil Found. 44 (1), 25–38.

Franzius, J.N., Potts, D.M., Burland, J.B., 2006. The response of surface structures to tunnel construction. Proc. Inst. Civil. Eng.: Geotech. Eng. 159 (1), 3–17.

Franzius, J.N., Potts, D.M., Burland, J.B., 2006. Twist behaviour of buildings due to tunnel induced ground movement. In: Kwast, E., Bakker, K., Broere, W., Bezuijen, A. (Eds.), Proceedings of the 5th International Conference on Geotechnical Aspects of Underground Construction in Soft Ground. Taylor and Francis, Amsterdam, pp. 107–113.

Giardina, G., Hendriks, M.A.N., Rots, J.G., 2010. Numerical analysis of tunnelling effects on masonry buildings: the influence of tunnel location on damage assessment. Adv. Mater. Res. 133, 289–294.

Giardina, G., Marini, A., Hendriks, M.A.N., Rots, J.G., Rizzardini, F., Giuriani, E., 2012. Experimental analysis of a masonry façade subject to tunnelling-induced settlement. Eng. Struct. 45, 421–434.

Giardina, G., Graaf, A.v.d., Hendriks, M.A.N., Rots, J.G., Marini, A., 2013. Numerical analysis of a masonry façade subject to tunnelling-induced settlement. Eng. Struct. 54, 234–247.

Giardina, G., Hendriks, M.A.N., Rots, J.G., 2015a. Sensitivity study on tunnelling induced damage to a masonry façade. Eng. Struct. 89, 111–129.

Giardina, G., Hendriks, M.A.N., Rots, J.G., 2015b. Damage functions for the vulnerability assessment of masonry buildings subjected to tunneling. J. Struct. Eng. 141 (9).

Goh, K.H., Mair, R.J., 2011. Building damage assessment for deep excavations in Singapore and the influence of building stiffness. Geotech. Eng. J. SEAGS AGSSEA 42 (3).

Guglielmetti, V., Grasso, P., Mahtab, A., Xu, S. (Eds.), 2008. Mechanized Tunnelling in Urban Areas: Design Methodology and Construction Control. Taylor and Francis.

Laefer, D.F., Hong, L.T., Erkal, A., Long, J.H., Cording, E.J., 2011. Manufacturing, assembly, and testing of scaled, historic masonry for one-gravity, pseudo-static, soil–structure experiments. Construct. Build. Mater. 25 (12), 4362–4373.

Liu, G., Houlsby, G.T., Augarde, C.E., 2000. 2-dimensional analysis of settlement damage to masonry buildings caused by tunnelling. Struct. Eng. 79 (1), 19–25.

Losacco, N., Burghignoli, A., Callisto, L., 2014. Uncoupled evaluation of the structural damage induced by tunnelling. Géotechnique 64, 646–656, 10.

Mair, R.J., 2003. Research on tunnelling-induced ground movements and their effects on buildings – lessons from the Jubilee Line Extension, keynote lecture. In: Jardine, F.M. (Ed.), Proceedings of International Conference on Response of Buildings to Excavation-induced Ground Movements, CIRIA Special Publication 199, RP620. Imperial College, London, UK, pp. 3–26.

Mair, R.J., 2013. Tunnelling and deep excavations: ground movements and their effects. In: Anagnostopoulos, A.E.A. (Ed.), Proceedings of the 15th European Conference on Soil Mechanics and Geotechnical Engineering – Geotechnics of Hard Soils – Weak Rocks (Part 4). IOS Press, pp. 39–70.

Mair, R.J., Taylor, R.N., 2001. Building response to tunnelling – case studies from construction of the Jubilee Line Extension, vol. 1. CIRIA special publication 200, London, 2001 (Ch. Elizabeth House: settlement predictions, pp. 195–215).

Mair, R.J., Taylor, R.N., Burland, J.B., 1996. Prediction of ground movements and assessment of risk of building damage due to bored tunnelling. In: Mair, R.J., Taylor, R.N. (Eds.), Proceedings of the International Symposium on Geotechnical Aspects of Underground Construction in Soft Ground. Balkema, Rotterdam, pp. 713–718.

Melis, M., Rodriguez Ortiz, J., 2001. Consideration of the stiffness of buildings in the estimation of subsidence damage by EPB tunnelling in the Madrid subway. In: Response of Buildings to Excavation Induced Ground Movements Conference. London.

Namazi, E., Mohamad, H., 2013. Assessment of building damage induced by three-dimensional ground movements. J. Geotech. Geoenviron. Eng. 139 (4), 608–618.

Netzel, H.D., 2009. Building Response Due to Ground Movements, Ph.D. thesis. Delft University of Technology.

Nghiem, H.L., Al Heib, M., Emeriault, F., 2014. Physical model for damage prediction in structures due to underground excavations. Tunnel. Under. Construct., 155–164

Pickhaver, J.A., Burd, H.J., Houlsby, G.T., 2010. An equivalent beam method to model masonry buildings in 3D finite element analysis. Comp. Struct. 88 (19–20), 1049–1063.

Potts, D.M., Addenbrooke, T.I., 1997. A structure's influence on tunnelling-induced ground movements. Proc. Inst. Civil Eng.: Geotech. Eng. 125 (2), 109–125.

Rampello, S., Callisto, L., Viggiani, G., Soccodato, F.M., 2012. Evaluating the effects of tunnelling on historical buildings: the example of a new subway in Rome/Auswertung der Auswirkungen des Tunnelbaus auf historische Gebäude am Beispiel einer neuen U-Bahnlinie in Rom. Geomech. Tunnel. 5 (3), 275–299.

Rots, J.G., 2000. Settlement damage predictions for masonry. In: Verhoef, L., Wittman, F. (Eds.), Maintenance and Restrengthening of Materials and Structures – Brick and Brickwork. Proceedings of the International Workshop on Urban Heritage and Building Maintenance. Aedificatio, Freiburg, pp. 47–62.

Skempton, A.W., MacDonald, D.H., 1956. The allowable settlements of buildings. Inst. Civil Eng. 5, 727–784.

Son, M., Cording, E.J., 2005. Estimation of building damage due to excavation-induced ground movements. J. Geotech. Geoenviron. Eng. 131 (2), 162–177.

Son, M., Cording, E.J., 2007. Evaluation of building stiffness for building response analysis to excavation-induced ground movements. J. Geotech. Geoenviron. Eng. 133 (8), 995–1002.

World Urbanization Prospects, 2014. The 2014 Revision, Highlights (ST/ESA/SER.A/352), Tech. rep., United Nations, Department of Economic and Social Affairs, Population Division.